Journal of Power Sources 246 (2014) 184–191

Contents lists available at ScienceDirect

Journal of Power Sources

journal homepage: www.elsevier.com/locate/jpowsour

Perfluoroalkyl-substituted ethylene carbonates: Novel electrolyte additives for high-voltage lithium-ion batteries

Ye Zhu [a], Matthew D. Casselman [b], Yan Li [a,c], Alexander Wei [b], Daniel P. Abraham [a,*]

[a] Chemical Sciences and Engineering Div., Argonne National Laboratory, 9700 S. Cass Ave., Argonne, IL 60439, USA
[b] Department of Chemistry, Purdue University, 560 Oval Drive, West Lafayette, IN 47907, USA
[c] Materials Science Program, University of Rochester, RC Box 270216, Rochester, NY 14627-0216, USA

HIGHLIGHTS

- A new family of perfluoroalkyl-substituted electrolyte additives is synthesized.
- Perfluorooctyl-substituted ethylene carbonate (PFO-EC) shows best improvements.
- PFO-EC improves capacity retention and lowers impedance rise in high voltage LIBs.
- PFO-EC shows beneficial effects on both positive and negative electrodes.
- LSV, XPS, and Raman spectroscopy are used to obtain diagnostic data.

GRAPHICAL ABSTRACT

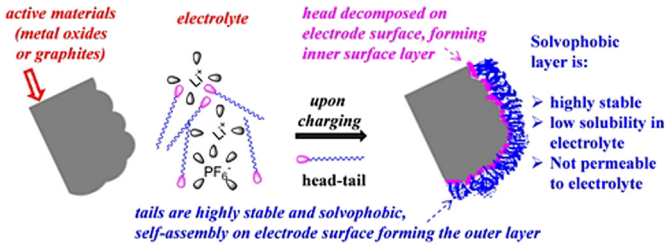

ARTICLE INFO

Article history:
Received 17 April 2013
Received in revised form
1 July 2013
Accepted 17 July 2013
Available online 25 July 2013

Keywords:
Polyfluoroalkyl compounds
Electrolyte additives
High voltage, high capacity
Lithium-ion battery
Solid electrolyte interphase (SEI)

ABSTRACT

A new family of polyfluoroalkyl-substituted ethylene carbonates is synthesized and tested as additives in lithium-ion cells containing EC:EMC + $LiPF_6$-based electrolyte. The influence of these compounds is investigated in $Li_{1.2}Ni_{0.15}Mn_{0.55}Co_{0.1}O_2$//graphite cells via a combination of galvanostatic cycling and electrochemical impedance spectroscopy (EIS) tests. Among the four additives studied in this work (4-(trifluoromethyl)-1,3-dioxolan-2-one (TFM-EC), 4-(perfluorobutyl)-1,3-dioxolan-2-one (PFB-EC), 4-(perfluorohexyl)-1,3-dioxolan-2-one (PFH-EC), and 4-(perfluorooctyl)-1,3-dioxolan-2-one (PFO-EC)), small amounts (0.5 wt%) of PFO-EC is found to be most effective in lessening cell performance degradation during extended cycling. Linear sweep voltammetry (LSV), X-ray photoelectron spectroscopy (XPS) and Raman spectroscopy are used to further characterize the effects of PFO-EC on the positive and negative electrodes. LSV data from the electrolyte, and XPS analyses of electrodes harvested after cycling, suggest that PFO-EC is oxidized on the cathode forming surface films that slow electrode/cell impedance rise. Differential capacity (dQ/dV) plots from graphite//Li cells suggest that PFO-EC is involved in solid electrolyte interphase (SEI) formation. Raman data from anodes after cycling suggest that structural disordering of graphite is reduced by the addition of PFO-EC, which may explain the improved cell capacity retention.

1. Introduction

High-capacity lithium- and manganese-rich metal oxides are gaining increased attention because of their ability to deliver high rechargeable capacities; when cycled between 2.0 and 4.7 V vs. Li, a rechargeable capacity of 270 mAh-g^{-1} can be routinely

* Corresponding author. Tel.: +1 630 252 4332.
E-mail addresses: zhuy@anl.gov (Y. Zhu), mdcassel@purdue.edu (M.D. Casselman), liy@anl.gov (Y. Li), alexwei@purdue.edu (A. Wei), abraham@anl.gov (D.P. Abraham).

0378-7753/$ – see front matter © 2013 Elsevier B.V. All rights reserved.
http://dx.doi.org/10.1016/j.jpowsour.2013.07.070

obtained [1]. Hence lithium-ion cells containing the Li_2MnO_3-stabilized $LiMO_2$ (M = Mn, Ni, Co) positive electrodes, graphite negative electrodes and EC:EMC (3:7 by wt.) + 1.2 M $LiPF_6$-based electrolyte (henceforth referred as Gen2 electrolyte) can be designed to meet the target cell specific capacity of 300 Wh kg^{-1} for transportation applications [2,3]. However, the target battery cycle life of up to 1000 charge–discharge cycles at 80% depth of discharge (DOD) can only be achieved through new electrolyte formulations because these cells show significant performance degradation on extended cycling [4]. Extensive diagnostic studies indicate that cell impedance rise mainly arises at the positive electrode, and cell capacity fade mainly results from lithium trapping in the solid electrolyte interphase (SEI) at the negative electrode [4–6]. During electrochemical aging, both electrodes undergo a cycle of surface film formation, decomposition, dissolution, and redeposition; this process results in the continuous consumption of lithium ions, thereby reducing cell capacity and often increasing cell impedance [7–9].

Electrolyte additives are known to be an effective and economic approach to improving the stability of electrode surface films [10]. In the past two decades, many organic and inorganic compounds have been identified as effective electrolyte additives: examples include vinylene carbonate (VC) [11,12], ethylene sulfite (ES) [13], vinyl ethylene carbonate (VEC) [14,15], and fluoroethylene carbonate (FEC) [16]. In recent years, with the emergence of many high-voltage cathode materials, the anodic stability of common electrolytes is recognized as the main bottleneck limiting the calendar- and cycle-life of high-energy lithium-ion cells [17]. Therefore, more attention has been devoted to improving stability of the cathode–electrolyte interface [6,18–25]. As part of DOE's Advanced Battery Research (ABR) program, we have been examining ways to mitigate performance degradation of cells containing $Li_{1.2}Ni_{0.15}Mn_{0.55}Co_{0.1}O_2$ ($0.5Li_2MnO_3 \cdot 0.5LiMn_{0.375}Ni_{0.375}Co_{0.25}O_2$)-based positive electrodes (LMR-NMC) that are cycled at voltages beyond 4.5 V versus Li. Initial studies indicate that common electrolyte additives such as VC, VEC, and FEC are not effective at enhancing long-term cycling performance of these cells, i.e. stable electrode passivation could not be achieved with traditional SEI-forming additives. This observation underscores the need for new electrolyte additives that effectively form stable electrode passivation films in high-energy and high-voltage lithium-ion cells.

Polyfluoroalkyl (PFA) compounds are well known for their high chemical stabilities, and exhibit both hydrophobic and lipophobic behaviors. Upon dispersing in organic solvents, solvophobic PFAs tend to aggregate and form micelles in solution [26]. These types of compounds have been extensively used as fluorosurfactants, and are especially valuable as additives in stain repellents [27]. In light of these facts, we envision that

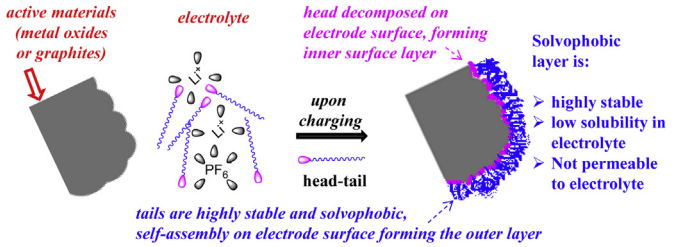

Scheme 1. Schematic representation illustrating the formation of double-layer passivation films via (i) decomposition of the headgroup on electrode surface forming an inner layer; (ii) self-assembly of tails on these inner layers forming a solvophobic outer layer.

compounds containing PFAs could serve as a new type of electrolyte additive, forming double-layered passivating layers that reduce both electrode surface degradation and electrolyte decomposition. In our design, the PFA additive has two components: (i) a reactive headgroup for attachment onto electrode surfaces via either reductive or oxidative decomposition, so that it becomes an integral part of the surface layer (inner layer); (ii) a polyfluoroalkyl chain that self-assembles on this inner layer as a solvophobic layer (outer layer) that is highly stable and impermeable to the electrolyte solvent. A schematic representation of this idea is shown in Scheme 1.

To explore this novel idea, we synthesized a series of PFA-substituted ethylene carbonates (PFA-EC) and studied them as electrolyte additives in our lithium-ion cells. Cell performance was characterized using a combination of galvanostatic cycling and electrochemical impedance spectroscopy (EIS) techniques, and supplemented by linear sweep voltammetry (LSV), X-ray photoelectron spectroscopy (XPS) and Raman spectroscopy data. Of the various PFA-EC compounds studied, we determined that perfluorooctyl-substituted ethylene carbonate (PFO-EC) most significantly improves the long-term cycling performance of our cells.

2. Experimental

2.1. Materials and synthesis

All chemicals used in the synthesis of polyfluoroalkyl compounds were purchased from commercial suppliers and used without further purification. 4-(trifluoromethyl)-1,3-dioxolan-2-one (TFM-EC) was purchased from Synquest Laboratories, Inc. (United States); all other polyfluoroalkyl-ECs were synthesized by a two-step reaction sequence (Scheme 2). Newly synthesized compounds were characterized by ^1H, ^{13}C, and ^{19}F NMR spectroscopy, using a 300- or 400-MHz spectrometer. All chemical shift values (δ) are reported in ppm, referenced relative to TMS (^1H and ^{13}C) or $CFCl_3$ (^{19}F).

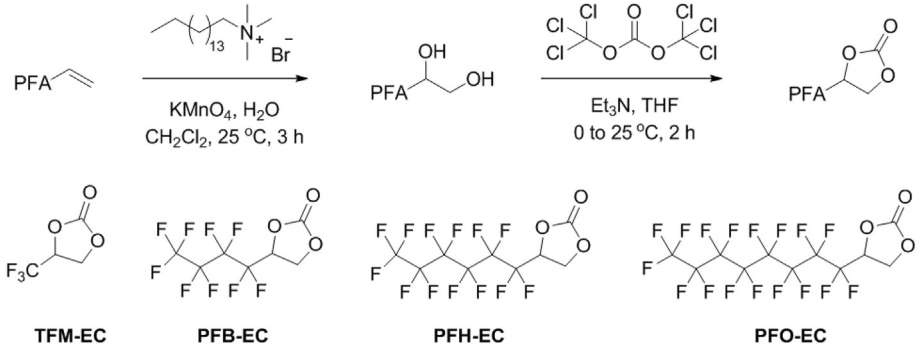

Scheme 2. Synthesis of polyfluoroalkyl (PFA)-substituted ethylene carbonates.

Table 1
Summary of $Li_{1.2}Ni_{0.15}Mn_{0.55}Co_{0.1}O_2$//graphite full cells cycling data using Gen2 electrolytes with or without various PFA-EC derivatives.

		Discharge capacity (mAh g(oxide)$^{-1}$)[a]		Capacity fade (mAh g^{-1}/percentage)	Capacity fade per cycle (mAh g^{-1})
		Initial	After 25 cycles		
Gen2	–	256.4	219.2	37.2/14.5%	1.49
TFM-EC	0.5 wt%	266.4	235.2	31.2/11.7%	1.25
	1 wt%	260.5	232.3	28.2/10.8%	1.13
PFB-EC	0.5 wt%	256.2	222.5	33.7/13.2%	1.35
	1 wt%	266.3	229.9	36.4/13.7%	1.46
PFH-EC	0.5 wt%	258.3	216.2	42.1/16.3%	1.68
	1 wt%	261.0	217.2	43.8/16.8%	1.75
PFO-EC	0.5 wt%	261.2	238.0	23.2/8.9%	0.93
	1 wt%	263.9	238.4	25.5/9.7%	1.02

[a] Cells were cycled between 2.2 and 4.6 V at 30 °C; the 15 mA g(oxide)$^{-1}$ current cycle data provide a good measure of "true capacity," as a low current minimizes ohmic polarization effects in capacity–voltage profiles.

In a typical synthesis, cetyltetramethylammonium bromide (350 mg, 0.96 mmol) and 1*H*,1*H*,2*H*-perfluorodecene (1.05 mL, 3.95 mmol) were dissolved in dichloromethane (50 mL), then treated with a 6.8% aqueous solution of potassium permanganate (100 mL). The biphasic reaction mixture was stirred vigorously for 3 h, then filtered through a pad of Celite and separated. The organic phase was washed with brine, dried over sodium sulfate, and concentrated. The residue was redissolved in acetone and passed through a silica gel plug, then concentrated to dryness to obtain 1*H*,1*H*,2*H*-perfluorodecane-1,2-diol as a white solid (0.94 g, 50%). The NMR characterization data for this compound are as follow: ^{1}H NMR (400 MHz, acetone-d_6): δ 4.28 (m, 1H), 4.02–3.67 (m, 2H). ^{13}C NMR (100 MHz, acetone-d_6): δ 122.7–108.3 (m), 71.49 (t, J = 22.6 Hz), 61.1 (s).

1*H*,1*H*,2*H*-perfluorodecane-1,2-diol (940 mg, 1.96 mmol) was dissolved in tetrahydrofuran (20 mL) and stirred at 0 °C, then treated sequentially with triethylamine (600 μL, 4.31 mmol) and triphosgene (210 mg, 0.71 mmol). The reaction mixture was warmed to room temperature over 2 h with stirring, then neutralized with saturated aqueous $NaHCO_3$. The product was extracted with diethyl ether, dried over sodium sulfate and concentrated, then recrystallized from chloroform to obtain PFO-EC as a white solid (785 mg, 79%). The NMR characterization data for this compound are as follow: ^{1}H NMR (400 MHz, acetone-d_6): δ 5.74 (m, 1H), 5.16–4.75 (m, 2H). ^{13}C NMR (100 MHz, acetone-d_6): δ 153.6 (s), 122.7–108.3 (m), 72.0 (dd, J = 22.2, 33.6 Hz), 64.4 (s). ^{19}F NMR (363 MHz, acetone-d_6): δ −78.1 (s, 3F), −116.6 to −127.2 (m, 14F).

Perfluorobutyl (PFB)- and perfluorohexyl (PFH)-substituted ECs were synthesized in a similar fashion from 1*H*,1*H*,2*H*-perfluorohexene and -octene respectively, in 48% and 62% overall yield. The NMR characterization data for these two compounds are as follow: *PFB-EC:* ^{1}H NMR (300 MHz, acetone-d_6): δ 5.82–5.65 (m, 1H), 5.00 (dd, 1H, J = 8.7, 9.7 Hz), 4.88 (dd, 1H, J = 4.7, 9.7 Hz). ^{13}C NMR (75 MHz, acetone-d_6): δ 153.81 (s), 122.8–108.1 (m), 72.1 (dd, J = 22.3, 33.6 Hz), 64.5 (s). *PFH-EC:* ^{1}H NMR (400 MHz, acetone-d_6) δ 5.83–5.65 (m, 1H), 4.99 (dd, 1H, J = 8.8, 9.6 Hz), 4.87 (dd, 1H, J = 4.7, 9.6 Hz). ^{13}C NMR (100 MHz, acetone-d_6): δ 153.64 (s), 122.6–108.4 (m), 72.0 (dd, J = 22.3, 33.7 Hz), 64.4 (s).

2.2. Electrochemical cycling tests and electrode surface characterization

The baseline electrolyte 1.2 M $LiPF_6$ in EC:EMC (3:7 by weight) (Gen2) is from Tomiyama Chemical Industry (Japan). The positive electrode comprises a 15 μm thick Al current collector coated with a composite of 86 wt% $Li_{1.2}Ni_{0.15}Mn_{0.55}Co_{0.1}O_2$, 6 wt% carbons (SuperP and SFG-6), and 8 wt% PVdF; the coating is 35 μm thick and the oxide loading is 6.6 mg cm^{-2}. The negative electrode comprises a 10 μm thick Cu current collector coated with a composite of ~90 wt% graphite, 4 wt% carbons (SuperP), and 6 wt% PVdF; the coating is 35 μm thick and the graphite loading is 5.6 mg cm^{-2}. Other details on cell components and chemistry can be found in a previous article [6].

The electrochemical anodic stability of electrolytes is examined by linear sweep voltammetry (LSV) using a three-electrode system. Platinum is used as the working electrode, and lithium metal as the counter and reference electrodes. LSV data are obtained at room temperature (23 °C) using a scan rate of 20 mV s^{-1} from the open circuit voltage (OCV) (ca. 3 V) to 5.5 V. The reduction behavior of electrolytes is investigated in graphite//Li coin cells. The onset potential of the reduction reaction, determined from the differential capacity curve (dQ/dV vs. V), is defined as the reduction potential.

Electrochemical cycling experiments are conducted in 2032-type coin cells, which are galvanostatically cycled at a constant temperature of 30 °C. The electrodes are weighed on an analytical balance (Mettler Toledo, XS105; 0.1 mg resolution) to confirm the active material loading. Formation cycling of full cells is conducted using a two-step protocol: three cycles between 2.2 and 4.1 V to enable complete wetting of the electrochemically active surfaces, followed by two cycles between 2.2 and 4.6 V to "activate" the oxide material; a 0.16 mA (~C/15 rate) current is used in both steps. Extended cycling in the 2.2–4.6 V voltage range is conducted with a higher current (0.8 mA, ~C/3 rate). Low current (0.16 mA) data are obtained periodically to monitor cell capacity because such cycling minimizes the effect of cell impedance. AC impedance measurements are conducted periodically with an EG&G 273A potentiostat

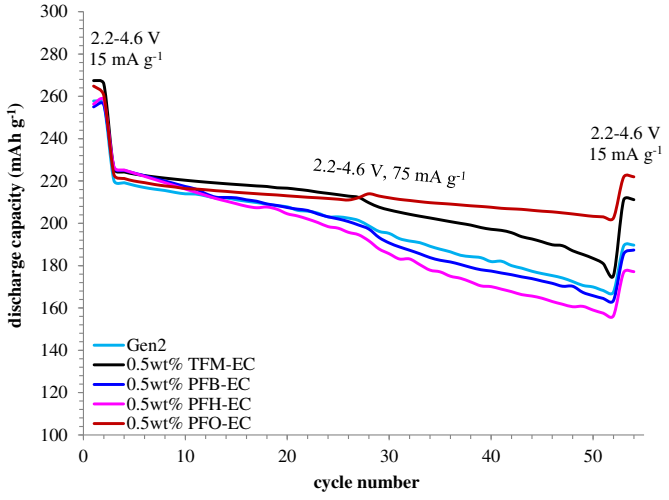

Fig. 1. Cell discharge capacity vs. cycle number plots for $Li_{1.2}Ni_{0.15}Mn_{0.55}Co_{0.1}O_2$// graphite full cells using Gen2 electrolytes with or without PFA-EC additives (0.5 wt%).

and a Solartron SI1260 frequency response analyzer controlled by ZPLOT measurement software. The cells are charged to 3.75 V and held for 4 h before data are collected in the potentiostatic mode, at 30 °C in the 100 kHz to 10 mHz frequency range, with a 10 mV perturbation around 3.75 V [28].

After the extended cycling, cells are discharged to, and held at, 2 V for 24 h before disassembly in an Ar-atmosphere glove box. The harvested electrodes are then examined by various electrochemical and physicochemical characterization tests. X-ray photoelectron spectroscopy (XPS) spectra on positive electrode samples are obtained with a Kratos Axis Ultra X-ray photoelectron spectrometer under ultrahigh vacuum (10^{-9} Torr) conditions and with monochromatic Al Kα (1486.6 eV) radiation as the primary excitation source. Survey spectra are collected at a constant pass energy of 160 eV from a ~1.0 mm^2 area of the sample. High-resolution spectra of the C1s, O1s, F1s, Li1s, P2p, and Mn2p core levels are collected at a pass energy of 20 eV and an energy step size of 100 meV with the same spot size. The acquired data are from a depth of ~2–5 nm from the electrode surface. Peak fits of all spectra are performed using the Shirley background correction and Gaussian–Lorentzian curve synthesis. The energy scale is adjusted based on the graphite peak in the C1s spectrum at 284.5 eV. Raman spectra on negative electrode samples were obtained on a Renishaw InVia Raman microscope using a 10-mW He–Ne laser (632 nm excitation). The power of the laser beam is adjusted to 1 mW at the sample. The acquired data are from a depth of ~1 μm from the electrode surface. The harvested electrodes are thoroughly rinsed in DMC and dried in the glove box prior to Raman measurements; this rinsing minimizes background fluorescence from electrolyte residue and electrode surface films.

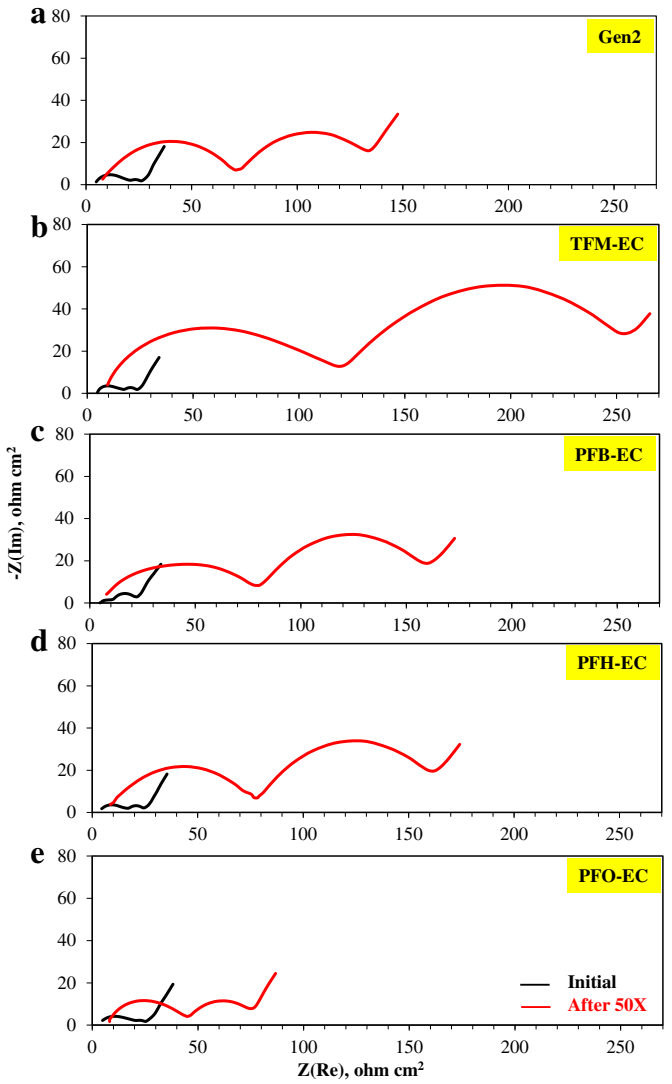

Fig. 2. AC impedance spectra of $Li_{1.2}Ni_{0.15}Mn_{0.55}Co_{0.1}O_2$//graphite full cells in (a) Gen2 electrolyte, and Gen2 electrolyte with 0.5wt% (b) TFM-EC, (c) PFB-EC, (d) PFH-EC, (e) PFO-EC cycled between 2.2 and 4.6 V at 30 °C after formation cycling (black lines) and after 50 cycles (red lines). (For interpretation of the references to colour in this figure legend, the reader is referred to the web version of this article.)

3. Results and discussion

3.1. Cycling performance of $Li_{1.2}Ni_{0.15}Mn_{0.55}Co_{0.1}O_2$//graphite full cells

During our cycling tests, cell to cell variations are always observed. These variations arise from various factors that include (i) small differences in active material weight between similar electrodes, (ii) small differences in the glove box environment when assembling the cells, (iii) differing amount of impurities in the electrolytes, additives, etc. However, the overall data trends observed across multiple cells are consistent. Therefore, only representative data and trends are reported here.

Table 1 summarizes the cycling performance of $Li_{1.2}Ni_{0.15}Mn_{0.55}Co_{0.1}O_2$//graphite full cells with various PFA-substituted ethylene carbonates (the corresponding capacity vs. cycle number plots can be found in the Supporting information). No obvious correlation is observed between cell cycling performance and PFA chain length. After 25 cycles, the capacity fade trends are as follows: PFH-EC > Gen2 ≥ PFB-EC > TFM-EC > PFO-EC. That is, relative to the baseline electrolyte, cells with the PFO-EC and PFH-EC additives show the best and worst capacity retention, respectively. Cell capacity retention shows a small but consistent correlation with the additive concentrations. TFM-EC cells with 1 wt% additive perform slightly better than those with 0.5 wt% additive, but cells with 0.5 wt% PFB-EC, PFH-EC and PFO-EC perform somewhat better than those with 1 wt% additive. Additional cells containing 0.5 wt% of each additive were tested to 50 cycles; the capacity fade data shown in Fig. 1 are consistent with the trend reported above.

AC impedance data of $Li_{1.2}Ni_{0.15}Mn_{0.55}Co_{0.1}O_2$//graphite full cells, without and with 0.5 wt% of each additive in the baseline

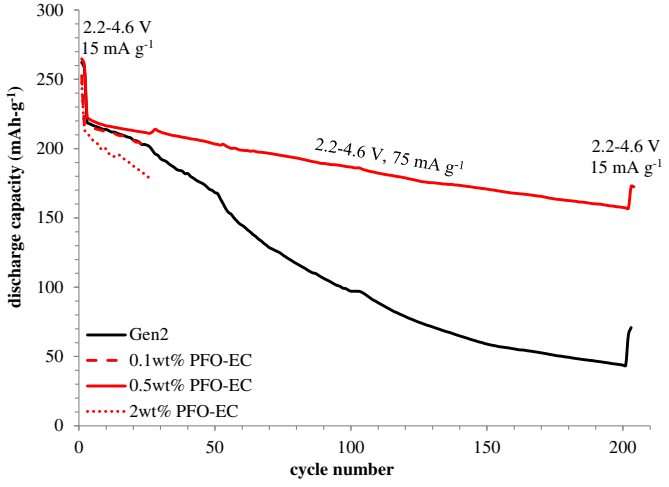

Fig. 3. Capacity vs. cycle number plots for $Li_{1.2}Ni_{0.15}Mn_{0.55}Co_{0.1}O_2$//graphite full cells with Gen2 electrolyte containing 0, 0.1, 0.5 and 2 wt% PFO-EC. Two low current (15 mA g(oxide)$^{-1}$) cycles precede and follow the rapid (75 mA g(oxide)$^{-1}$) aging cycles.

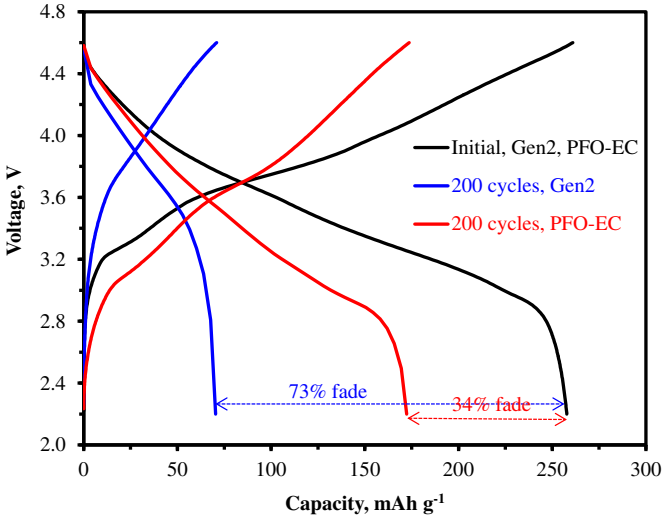

Fig. 4. Capacity–voltage plots for full cells containing the Gen2 electrolyte and Gen2 + 0.5 wt% PFO-EC electrolyte. The data were acquired with a 15 mA g(oxide)$^{-1}$ current in the 2.2–4.6 V voltage window at 30 °C. The initial cycle data are similar for cells with and without the additive.

electrolyte, are shown in Fig. 2. The data for various cells are very similar after the initial formation cycling. After 50 cycles, however, cell impedances are significantly different and show the following trend: TFM-EC > PFH-EC ≥ PFB-EC > Gen2 > PFO-EC. That is, cells with 0.5 wt% TFM-EC and 0.5wt% PFO-EC show the highest and lowest impedances, respectively.

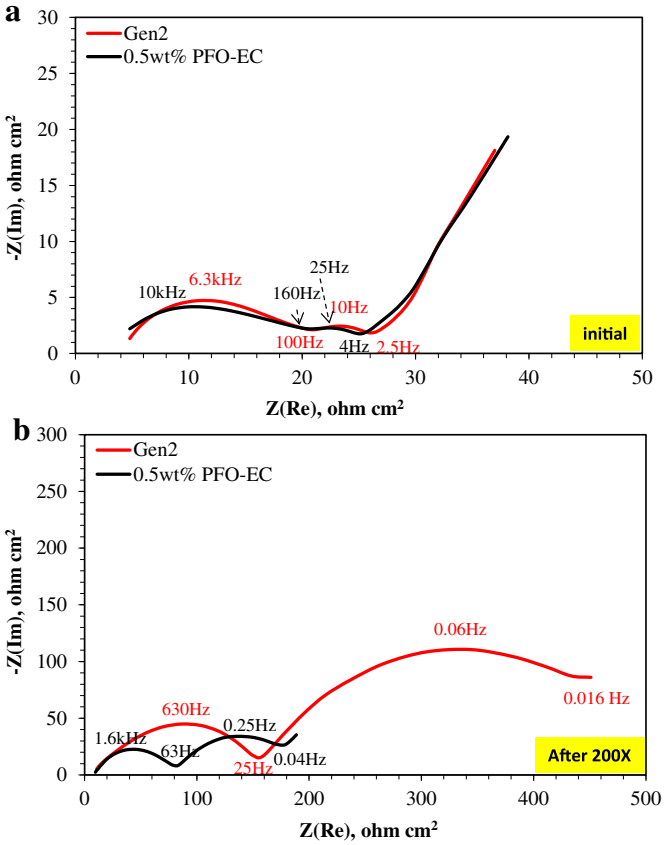

Fig. 5. AC impedance spectra of $Li_{1.2}Ni_{0.15}Mn_{0.55}Co_{0.1}O_2$//graphite full cells, with and without 0.5 wt% PFO-EC, after (a) formation cycles, (b) 200 cycles at 30 °C.

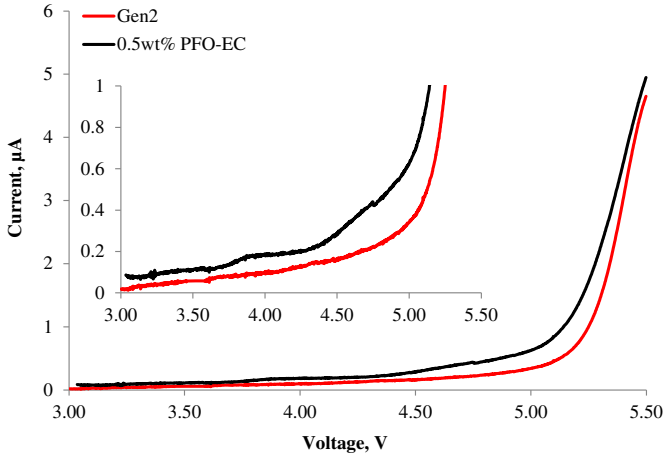

Fig. 6. Oxidation behavior of Gen2 electrolyte (1.2 M $LiPF_6$ in 3:7 EC:EMC by wt.), with and without PFO-EC, determined by linear sweep voltammetry (LSV) at a Pt working electrode. The inset contains an expanded view of the data.

Of all the additives tested, cells with PFO-EC provided the best performance, which we attribute to a more solvophobic barrier and better protection of the electrode surfaces. In fact, PFO-EC is the least soluble in the Gen2 electrolyte; the maximum additive

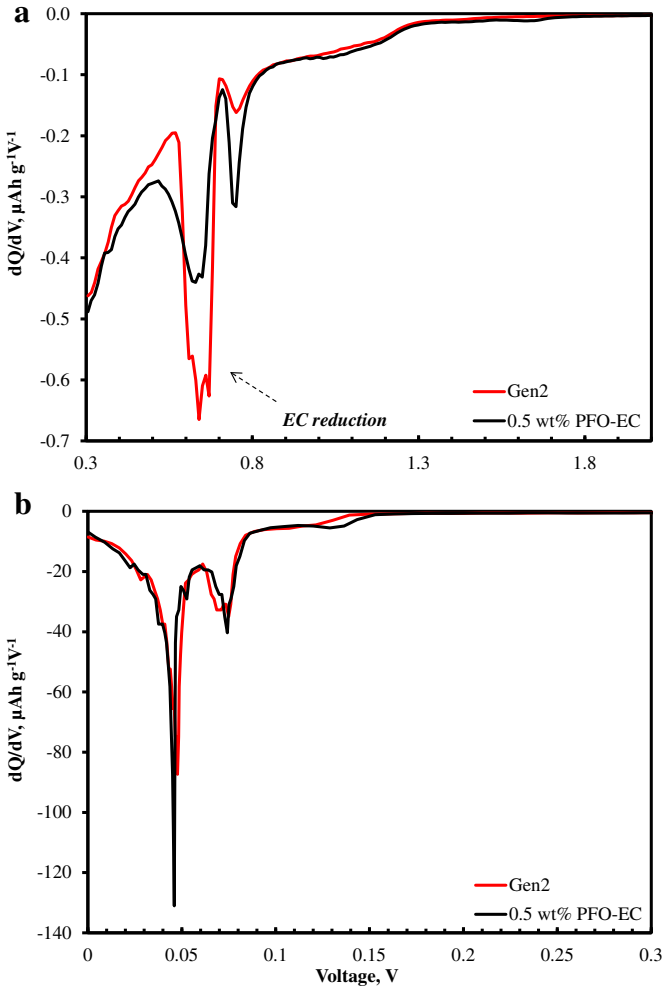

Fig. 7. Differential capacity plots from first cycle lithiation data of graphite//Li cells in Gen2 electrolyte with and without PFO-EC. (a) The *X*-axis voltage range is from 2 to 0.3 V, which highlights electrolyte reduction processes; (b) the *X*-axis voltage range is from 0.3 to 0 V, which shows the main graphite lithiation peaks.

loading is ca. 2 wt%, whereas loadings of PFH-EC, PFB-EC and TFM-EC could be as high as 5 wt%. The lower solubility of PFO-EC suggests that its decomposition products may also be less soluble in the electrolyte, which would lend greater stability to the electrode surface films. In contrast, electrode surface films arising from PFH-EC, PFB-EC and TFM-EC are less stable (or more soluble), and hence less beneficial to cell performance.

It should be noted that variation in molecular weights of the PFA-EC additives give rise to large differences in molar ratios for a given wt.% loading; for example, the molar equivalents of PFO-EC, PFH-EC, PFB-EC, and TFM-EC are 1.00, 1.25, 1.65, and 3.25, respectively. The improved capacity retention of TFM-EC cells might thus relate to an effectively higher molarity; previous work has shown that TFM-EC forms an effective SEI on a graphite anode [29]. Indeed, when the concentration of TFM-EC is reduced to 0.25 wt% (a closer molar ratio to 0.5 wt% PFO-EC), a faster cell capacity fade is observed (data not shown).

A systematic study was further conducted to determine the concentration of PFO-EC that provide the best performance. Fig. 3 shows that $Li_{1.2}Ni_{0.15}Mn_{0.55}Co_{0.1}O_2$//graphite full cells with 0.5 wt % PFO-EC provide the best capacity retention. Cells with 2 wt% PFO-EC show a faster capacity fade, whereas performance of cells with 0.1 wt% PFO-EC is similar to that of the baseline cell. After 200 cycles, the discharge capacity of cells with 0.5 wt% PFO-EC is 172 mAh-g^{-1}, which is 66% of its initial discharge capacity (260 mAh-g^{-1}). In contrast, the discharge capacity of the baseline (Gen2 only) cells is 70 mAh-g^{-1}, which is 27% of its initial discharge capacity (258 mAh-g^{-1}). The enhanced capacity retention resulting from the additive is also clearly seen in Fig. 4, which contains capacity–voltage data from the full cells. The PFO-EC additive is also effective at inhibiting cell impedance rise during long-term cycling. Fig. 5a shows that cells with 0.5 wt% PFO-EC have similar impedances as baseline cells after the initial cycling. However, after 200 cycles between 2.2 and 4.6 V (Fig. 5b), the impedance of the PFO-EC bearing cell is much smaller than that of the Gen2 baseline cell. Our previous studies have indicated that cell impedance rise in $Li_{1.2}Ni_{0.15}Mn_{0.55}Co_{0.1}O_2$//graphite full cells occurs primarily at the positive electrode [4]. The reduced full cell impedance for the PFO-EC-containing cells suggests that the additive forms effective surface films at this electrode.

3.2. Oxidation–reduction behavior of PFO-EC cells

Fig. 6 shows the oxidation LSV plot of a Pt electrode in Gen2 electrolyte, with and without PFO-EC. For the baseline electrolyte, accelerated current increase is seen only at voltages greater than 4.8 V, whereas the PFO-EC bearing electrolyte shows an oxidation current increase starting near ~4.3 V. The higher oxidation current suggests that the PFO-EC has a lower oxidation potential than Gen2 electrolyte and could be sacrificially oxidized on the positive electrode.

Differential capacity (dQ/dV) plots for the first lithiation cycle of graphite//Li cells were obtained to study electrolyte reduction behavior, without or with 0.5 wt% PFO-EC in the electrolyte (Fig. 7). The dQ/dV plots were quite similar regardless of PFO-EC, and additional reduction peaks at higher voltages (>1 V vs Li^+/Li) were not observed (Fig. 7a). Increasing the PFO-EC concentration to 2 wt % yielded similar results (data not shown). The PFO-EC cells showed a larger peak at ~0.75 V vs. Li^+/Li and a smaller peak at ~0.65 V vs Li^+/Li, compared to the Gen2 cells, which suggests that the additive modifies electrolyte reduction behavior. This may be due in part to the sacrificial reduction of PFO-EC on the graphite anode surface, at

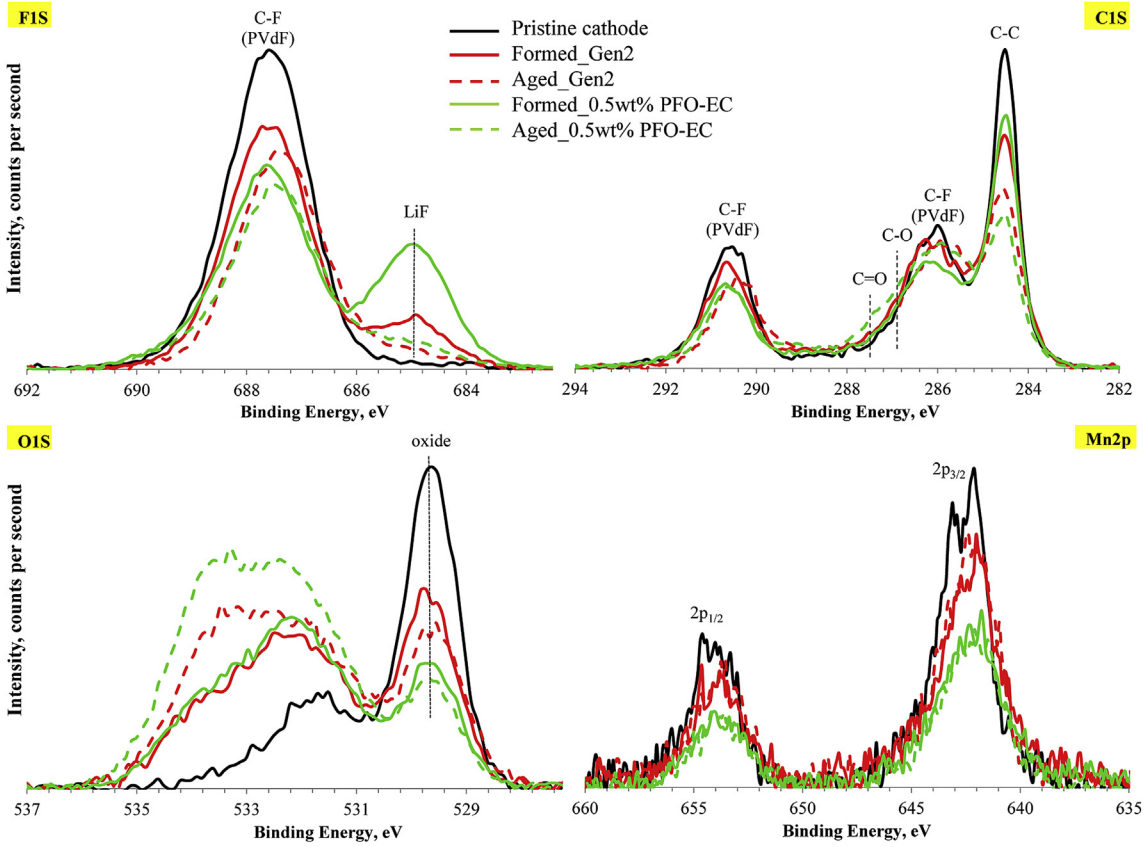

Fig. 8. XPS spectra from a pristine positive electrode and harvested positive electrodes from $Li_{1.2}Ni_{0.15}Mn_{0.55}Co_{0.1}O_2$//graphite full cells containing Gen2 electrolyte, with and without 0.5 wt% PFO-EC, after formation cycling and after aging. The aged cells underwent 200 cycles at 30 °C, between 2.2 and 4.6 V, with 75 mA g^{-1} current.

a similar reduction potential as EC [30]; however, the data does not provide unequivocal proof, as the PFO-EC carbonyl is relatively more electrophilic and may also be involved in SEI formation through some chemical reactions. In particular, it is possible that PFO-EC can preferentially react with various nucleophiles generated from EC reduction (alkoxides, carbonates, etc.), contributing to SEI formation via anionic polymerizations [31]. The resulting SEI, composed of PFO-EC reaction products, could be considered as a "functionalized" passivation film with low solvent permeability, which may improve the SEI layer stability and cell capacity retention. Moreover, this SEI does not affect the overpotential for lithium ion reduction and intercalation compared to the SEI formed in the additive-free electrolyte (Fig. 7b).

3.3. XPS spectra from fresh and harvested positive electrodes

XPS spectra from the pristine positive electrode, and from positive electrodes harvested from formed and aged full cells with and without 0.5 wt% PFO-EC, are shown in Fig. 8. The harvested electrodes were lightly rinsed with anhydrous DMC to remove residual electrolyte. Element concentrations (at.%) calculated from the data are shown in Table 2.

The C1s spectra of the pristine electrode reveals peaks arising from the poly(vinylidene fluoride) (PVdF) binder (285.8 eV, 290.9 eV) and the conductive carbons (284.5 eV). These peak intensities are reduced in cathodes harvested after formation cycling and continue to decrease with further cycling/aging, indicative of surface films growth on the electrode surfaces. Similar trends are observed in the O1s, F1s and Mn2p spectra: upon cycling, intensities are reduced for the F1s peak (687.8 eV) corresponding to PVdF, and for the O1s peak (529.6 eV) and Mn2p3/2 and Mn2p3/2 peaks (642.1 eV, 654.2 eV) corresponding to the metal oxide. In all cases, these peak reductions are somewhat greater for the samples containing PFO-EC, which suggests thicker electrode surface films. However, the thicker films do not excessively impede lithium-ion motion, as the impedance of aged PFO-EC cells is much lower than that of cells without the additive (Fig. 5b).

The peak centered at 685 eV in the F1s spectra is from LiF, which is present on both electrodes from the Gen2 and PFO-EC-containing cells after formation cycling, but is stronger in the latter case. We attribute the higher LiF content to the oxidation of PFO-EC, which is consistent with our observations from the LSV study (Fig. 6). This observation is important because the similar initial cell impedances of the Gen2 and PFO-EC cells (Fig. 5a) indicate that cell impedance rise cannot be solely attributed to the presence of LiF. Upon further cycling, the LiF peak intensities decrease for both samples, which could simply be due to growth of the overlying layers.

Table 2 and the O1s spectra show that the oxygen content in the electrode surfaces increases slightly after formation cycling but more significantly after extended cycling: the most obvious changes are in the 531–535 eV range. These O1s intensity changes, along with C1s intensity increases in the 286–290 eV range, suggest the presence of various species that may include alkoxides, carbonyls and carbonates; peaks arising from these compounds overlap with the PVdF peaks, which makes definitive identification difficult. Table 2 also shows that the P content in electrode surface films increases upon cycling/aging for both Gen2 and PFO-EC samples. In addition, the P2p spectra shows an increase in the intensity of peaks centered around 134.6 eV (see Supporting information), which indicate the presence of P–O bonds that may arise from $Li_xPO_yF_z$ compounds; intensity from these species would also be seen in the O1s data.

Table 2
Element concentrations (at.%) calculated from XPS spectra of the fresh positive electrode and from positive electrode samples harvested from cells that were formed and aged in the Gen2 and Gen2+0.5 wt% PFO-EC electrolytes.

	C 1s	F 1s	O 1s	Li 1s	Mn 2p	P 2p
Fresh	58.5	26.5	9.7	3.3	1.5	0
Formed_Gen2	53.7	22.7	11.6	9.3	1.4	0.97
Aged_Gen2	54.6	21.8	15.7	3.8	1.6	1.9
Formed_PFO-EC	47.8	24.8	10.4	14.6	0.94	1.4
Aged_PFO-EC	56.1	20.8	17.9	1.7	0.98	2.5

3.4. Raman spectra from fresh and harvested negative electrodes

The graphite anodes were examined by Raman spectroscopy, a standard tool for characterizing carbonaceous materials [32,33]. Fig. 9 shows representative Raman data from pristine and harvested negative electrodes; in all spectra, three peaks appear between 1000 and 2000 cm^{-1}, assignable as the D, G, and D′ bands (~1350, ~1580, and ~1620 cm^{-1} respectively). The G band is a commonly accepted signature of graphitic carbon, whereas the D and D′ bands are associated with defects and disorder within

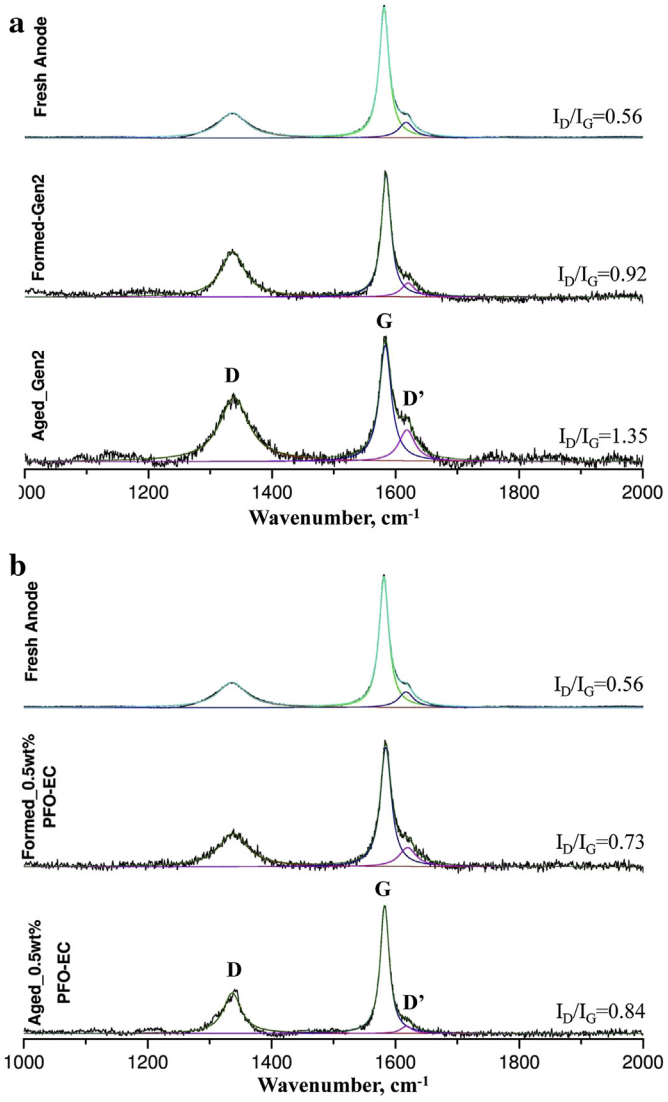

Fig. 9. Raman spectra from graphite electrodes, before and after exposure to Gen2 electrolyte or Gen2+0.5 wt% PFO-EC (a and b, respectively). Electrodes were harvested from cells cycled between 2.2 and 4.6 V, either after formation cycles ("formed") or after 200 cycles ("aged"). Band intensities are normalized to the G-band.

graphite; the ratio of the D and G band areas (I_D/I_G) correlates with increased carbon disorder.

Fig. 9a shows the Raman spectra for graphite electrodes harvested from cells cycled in Gen2 electrolyte. The I_D/I_G for the pristine graphite electrode is 0.56, which is higher than that expected for pure graphite ($I_D/I_G = 0$) due to the presence of granular carbons ($I_D/I_G = 2.47$). The D and G peak shapes change noticeably for anode samples after formation cycling ($I_D/I_G = 0.92$) and even more after another 200 cycles ($I_D/I_G = 1.35$), with a substantial increase in the size of the D peak and a broadening of the G peak. These data suggest structural disordering at the graphite surface, which exposes new graphitic edges and fragments of graphite planes that catalyze reductive decomposition of the electrolyte. Continued structural disordering upon prolonged cycling contributes toward increased electrolyte reduction and SEI reformation, leading to gradual transfer of lithium from the cathode to the anode SEI and eventually degrading cell capacity. Fig. 9b shows Raman spectra for the fresh graphite electrode and for harvested electrodes from cells cycled in the PFO-EC electrolyte; the I_D/I_G is 0.73 after formation cycling and 0.84 after 200 cycles. These data suggest that the PFO-EC additive reduces disordering of the graphite surface, both after formation cycling and after extended cycling, which results in less Li^+ trapping and improved cell capacity retention.

4. Conclusions

A new family of polyfluoroalkyl-substituted ECs is examined as electrolyte additives in full cells using $Li_{1.2}Ni_{0.15}Mn_{0.55}Co_{0.1}O_2$-based cathodes and graphite anodes. Addition of 0.5 wt% 4-(perfluorooctyl)-1,3-dioxolan-2-one (PFO-EC) to a standardized electrolyte solution, Gen 2 (1.2 M $LiPF_6$ in a 3:7 mixture of EC:EMC), is found to improve capacity retention and reduce impedance rise in full cells cycled between 2.2 and 4.6 V. The LSV and XPS data suggest that PFO-EC is sacrificially oxidized on the positive electrode; the dQ/dV plots from the first lithiation cycle of graphite//Li cells also suggest that PFO-EC is involved in SEI formation.

Improvements in cell performance from the PFO-EC additive can be attributed to synergistic effects of the performance on both electrodes. The sacrificial oxidation of PFO-EC at the cathode forms surface films that reduce cell impedance rise; PFO-EC also reacts at the anode to generate a more stable SEI. The two mechanisms are synergistic in their actions: the cathode protection not only reduces electrolyte oxidation and slows down cell impedance rise, but also reduces the dissolution of transition metal from the oxide, and ultimately helps to improve SEI stability at the negative electrode. At the anode, PFO-EC stabilization of the SEI lessens electrolyte reduction and lithium trapping, which helps to maintain electrolyte integrity and reduce cell impedance rise. Further mechanistic studies on additive oxidation–reduction reactions are currently underway, and will be discussed in due course.

The data presented here validates our hypothesis of using polyfluoroalkyl-ECs as novel functional electrolyte additives, and opens up possibilities for developing other PFA-substituted additives that may provide further performance improvements. These PFA-substituted compounds may also be useful additives in other lithium-ion cells, including those based on the 5 V spinel-based positive electrodes.

Acknowledgments

Support from the U.S. Department of Energy's Vehicle Technologies Program, specifically from Dave Howell and Peter Faguy, is gratefully acknowledged. The submitted manuscript has been created by UChicago Argonne, LLC, Operator of Argonne National Laboratory ("Argonne"). Argonne, a U.S. Department of Energy Office of Science laboratory, is operated under Contract No. DE-AC02-06CH11357. We are grateful to B. Polzin, A. Jansen, and S. Trask from the U.S. Department of Energy's (DOE) Cell Fabrication Facility (CFF), Argonne National Laboratory for providing electrodes used in this work. The CFF is fully supported by the DOE Vehicle Technologies Program (VTP) within the core funding of the Applied Battery Research (ABR) for Transportation Program. We acknowledge use of the Center for Microanalysis of Materials (CMM) at the Frederick Seitz Materials Research Laboratory, University of Illinois at Urbana-Champaign (Illinois). Use of the Center for Nanoscale Materials at Argonne, was supported by the U. S. Department of Energy, Office of Science, Office of Basic Energy Sciences, under Contract No. DE-AC02-06CH11357.

Appendix A. Supplementary data

Supplementary data related to this article can be found at http://dx.doi.org/10.1016/j.jpowsour.2013.07.070.

References

[1] M.M. Thackeray, S.-H. Kang, C.S. Johnson, J.T. Vaughey, R. Benedek, S.A. Hackney, J. Mater. Chem. 17 (2007) 3112–3125.
[2] J.M. Tarascon, Philos. Transact A Math. Phys. Eng. Sci. 368 (2010) 3227–3241.
[3] M.M. Thackeray, C. Wolverton, E.D. Isaacs, Energy Environ. Sci. 5 (2012) 7854–7863.
[4] Y. Li, M. Bettge, B. Polzin, Y. Zhu, M. Balasubramanian, D.P. Abraham, J. Electrochem. Soc. 160 (2013) A3006–A3019.
[5] M. Bettge, Y. Li, B. Sankaran, N.D. Rago, T. Spila, R.T. Haasch, I. Petrov, D.P. Abraham, J. Power Sources 233 (2013) 346–357.
[6] Y. Zhu, Y. Li, M. Bettge, D.P. Abraham, J. Electrochem. Soc. 159 (2012) A2109–A2117.
[7] Y.S. Cohen, Y. Cohen, D. Aurbach, J. Phys. Chem. B 104 (2000) 12282–12291.
[8] K. Tasaki, A. Goldberg, J.-J. Lian, M. Walker, A. Timmons, S.J. Harris, J. Electrochem. Soc. 156 (2009) A1019–A1027.
[9] J. Li, A.K. Dozier, Y. Li, F. Yang, Y.-T. Cheng, J. Electrochem. Soc. 158 (2011) A689–A694.
[10] S.S. Zhang, J. Power Sources 162 (2006) 1379–1394.
[11] Y. Wang, S. Nakamura, K. Tasaki, P.B. Balbuena, J. Am. Chem. Soc. 124 (2002) 4408–4421.
[12] J.-Y. Eom, I.-H. Jung, J.-H. Lee, J. Power Sources 196 (2011) 9810–9814.
[13] H. Sano, H. Sakaebe, H. Matsumoto, J. Electrochem. Soc. 158 (2011) A316–A321.
[14] T.-H. Nam, E.-G. Shim, J.-G. Kim, H.-S. Kim, S.-I. Moon, J. Electrochem. Soc. 154 (2007) A957–A963.
[15] Y. Hu, W. Kong, H. Li, X. Huang, L. Chen, Electrochem. Commun. 6 (2004) 126–131.
[16] Y. Domi, M. Ochida, S. Tsubouchi, H. Nakagawa, T. Yamanaka, T. Doi, T. Abe, Z. Ogumi, J. Electrochem. Soc. 159 (2012) A1292–A1297.
[17] L. Hu, Z. Zhang, K. Amine, J. Power Sources 236 (2013) 175–180.
[18] M. Hu, X. Pang, Z. Zhou, J. Power Sources 237 (2013) 229–242.
[19] M. Xu, Y. Liu, B. Li, W. Li, X. Li, S. Hu, Electrochem. Commun. 18 (2012) 123–126.
[20] C.A. von, K. Xu, J. Electrochem. Soc. 158 (2011) A337–A342.
[21] J.-N. Lee, G.-B. Han, M.-H. Ryou, D.J. Lee, S. Jongchan, J.W. Choi, J.-K. Park, Electrochim. Acta 56 (2011) 5195–5200.
[22] S. Dalavi, M. Xu, B. Knight, B.L. Lucht, Electrochem. Solid-State Lett. 15 (2012) A28–A31.
[23] Y. Zhu, Y. Li, M. Bettge, D.P. Abraham, Electrochim. Acta (2013), http://dx.doi.org/10.1016/j.electacta.2013.1003.1102.
[24] Q. Wu, W. Lu, M. Miranda, T.K. Honaker-Schroeder, K.Y. Lakhsassi, D. Dees, Electrochem. Commun. 24 (2012) 78–81.
[25] Z. Zhang, L. Hu, H. Wu, W. Weng, M. Koh, P.C. Redfern, L.A. Curtiss, K. Amine, Energy Environ. Sci. 6 (2013) 1806–1810.
[26] H.-J. Lehmler, Chemosphere 58 (2005) 1471–1496.
[27] R. Renner, Environ. Sci. Technol. 40 (2006) 12–13.
[28] K.G. Gallagher, S.-H. Kang, S.U. Park, S.Y. Han, J. Power Sources 196 (2011) 9702–9707.
[29] X.J. Wang, H.S. Lee, H. Li, X.Q. Yang, X.J. Huang, Electrochem. Commun. 12 (2010) 386–389.
[30] S.H. Kang, D.P. Abraham, A. Xiao, B.L. Lucht, J. Power Sources 175 (2008) 526–532.
[31] G. Gachot, S. Grugeon, M. Armand, S. Pilard, P. Guenot, J.-M. Tarascon, S. Laruelle, J. Power Sources 178 (2008) 409–421.
[32] R. Kostecki, F. McLarnon, J. Power Sources 119–121 (2003) 550–554.
[33] E. Markervich, G. Salitra, M.D. Levi, D. Aurbach, J. Power Sources 146 (2005) 146–150.